

Adjoint computation of Berry phase gradients

Cyrill Bösch^{1,2*}, Marc Serra-Garcia², Christian Böhm¹, Andreas Fichtner¹

¹Institute of Geophysics, ETH Zurich, Sonneggstrasse 5, 8092 Zurich, Switzerland.

²Department of Computer Science, Princeton University, 35 Olden Street, Princeton, NJ 08540, US.

³AMOLF, Science Park 104, 1098 XG Amsterdam, Netherlands.

*Corresponding author(s). E-mail(s): cb7454@princeton.edu;

Contributing authors: M.SerraGarcia@amolf.nl; christian.boehm@eaps.ethz.ch;
andreas.fichtner@eaps.ethz.ch;

Abstract

Berry phases offer a geometric perspective on wave propagation and are key to designing materials with topological wave transport. However, controlling Berry phases is challenging due to their dependence on global integrals over the Brillouin zone, making differentiation difficult. We present an adjoint-based method for efficiently computing the gradient of the Berry phase with respect to system parameters, involving only one forward and one adjoint calculation. This approach enables the use of advanced optimization techniques, such as topology optimization, to design new materials with tailored topological wave properties.

Keywords: Berry phases, Topology, Inverse design, Adjoint method

1 Introduction

The introduction of geometric phases to explain wave phenomena can be attributed to Sir Michael Berry's groundbreaking paper, "Quantal phase factors accompanying adiabatic changes" [1]. These phases exhibit an inherent robustness as they only depend on the geometry of the path. Furthermore, in topological systems like the Su-Schrieffer-Heeger model, the Berry phase predicts the existence or absence of topological wave states. The field of topological physics was born with the observation and the explanation of the quantum Hall effect [2, 3]. Since then, geometric phases and topology have played a revolutionary role in multiple domains of physics, such as condensed matter physics [4, 5, 6, 7, 8, 9, 10, 11], topological photonic [12, 13, 14, 15, 16, 17, 18,

19, 20, 21, 22, 23, 24] and phononic metamaterials [25, 26, 27, 28, 29, 30, 31, 32, 33, 34, 35, 36, 37, 38, 39, 40, 41, 42, 43, 44, 45], quantum holonomic computing [46, 47, 48, 49], the control and guiding of light [50, 51, 52, 53, 54, 55] and seismology [56, 57].

Recent developments in the field have shifted from fundamental research to exploiting these phenomena to invent new devices. For instance, quantum devices for signal processing, which leverage geometric phases as information carriers, have been introduced [58, 59, 60, 61, 62], topological states are harnessed to robustly propagate information [63, 64, 65, 66], and waveguides are designed based on the accumulation of a geometric phase as a wave packet is passed through a wave plate [67, 53, 50]. Of particular interest is the

design of topological metamaterials [68, 39, 40, 69, 70, 71, 72, 73, 74, 75, 76, 77, 76] which is inherently challenging due to the intrinsic robustness of topological systems resulting from the fact that the topology of a material is invariant with respect to a large class of model perturbations. The design of these devices has predominantly been steered by intuition or top-down strategies, optimizing the desired output (e.g. the localization of energy at a specific location) rather than directly addressing the topological invariant.

In contrast, in our recent study [78], we showed that topological invariants can be tuned using the concept of symmetry relaxation. This approach de-quantizes the invariant and allows a system to be systematically steered through a topological phase transition by following the gradient of the smoothed topological invariant with respect to design or control parameters.

In this study, we present an efficient method to compute gradients of Berry phases which often act as topological invariants in these systems. To this end, we employ the adjoint method [79, 80, 81, 82, 83] from the domain of PDE-constrained optimization. The adjoint method allows us to efficiently compute gradients, especially when the design space that characterises the device or material is high dimensional such as when optimizing continuous fields. The large design space renders the use of sampling algorithms or finite differentiation impractical. Such expansive design spaces are commonly encountered in the design of application devices, e.g., through topology optimization [84], contrasting with low-dimensional systems such as tight-binding or mass spring models. Additionally, augmenting the number of design variables may allow us to identify designs with enhanced performance and robustness. The method introduced here can also be integrated in multi-objective optimization scenarios where, in addition to the Berry phase, one also optimizes, e.g., the quality factor or the operational bandwidth of topological states [76].

In a context broader than just topological invariants, the method is readily applicable to any single-band or multiband, non-Abelian geometric phase resulting from either cyclic or non-cyclic adiabatic evolutions, steered by either a Hermitian quantum-like first-order or a classical-like second-order dynamical system and variants that can be mapped to either of the two.

In Section 2, we review the emergence of the Berry phase in both adiabatic quantum and classical systems, and state the gradient problem addressed in this article. In Section 3, we derive the adjoint method, apply it to an elastic metamaterial crystal and provide a complexity analysis. Section 4 discusses the generalization to multi-band Berry phases, derived from the Wilson loop eigenvalues. Finally, we conclude in Section 5.

2 Preliminaries: quantum and classical Berry phases

We consider a discrete Hermitian non-autonomous quantum system whose dynamics are governed by a quantum Hermitian Hamiltonian, $\mathbf{H}(\mathbf{p}_H, t) \in \mathbb{C}^{N \times N}$, where N is the state space dimension; or a classical system defined by a Hermitian mass matrix, $\mathbf{M}(\mathbf{p}_M) \in \mathbb{C}^{N \times N}$, and a Hermitian stiffness matrix, $\mathbf{K}(\mathbf{p}_K, t) \in \mathbb{C}^{N \times N}$. Without loss of generality, the N_X parameters of the matrices, $\mathbf{p}_X \in \mathbb{R}^{N_X}$, are assumed to be real. The evolution of a quantum state $\mathbf{y} \in \mathbb{C}^N$ is given by the solution of the time-dependent Schrödinger equation

$$i\partial_t \mathbf{y}(t) = \mathbf{H}(\mathbf{p}_H, t)\mathbf{y}(t). \quad (1)$$

The corresponding instantaneous eigenvalue problem is

$$E_n(t)\mathbf{n}(t) = \mathbf{H}(\mathbf{p}_H, t)\mathbf{n}(t), \quad (2)$$

where $(E_n(t), \mathbf{n}(t))$ are the n -th instantaneous eigenvalue or energy and orthonormal eigenvector of $\mathbf{H}(\mathbf{p}_H, t)$. If $E_n(t)$ is non-degenerate for all integration times and the evolution of the Hamiltonian is slow enough in comparison to the energy gap, then a state initialized in the n -th eigenstate, i.e., $\mathbf{y}(0) = \mathbf{n}(0)$, remains in it and accumulates two types of phases [85, 86, 87]:

$$\mathbf{y}(t) \approx e^{-i\hat{E}_n(t)} e^{-i\theta_n(t)} \mathbf{n}(t), \quad (3)$$

where $\hat{E}_n(t)$ is the dynamical phase, computed as

$$\hat{E}_n(t) = \int_0^t E_n(t') dt', \quad (4)$$

and $\theta_n(t)$ is the geometric phase, or Berry phase, which is obtained as

$$\theta_n(t) = \text{Im} \int_0^t \langle \mathbf{n}(t') | \partial_t \mathbf{n}(t') \rangle dt'. \quad (5)$$

The inner product is given by $\langle \mathbf{a} | \mathbf{b} \rangle = \sum_{i=1}^N a_i^* b_i$, and $*$ denotes complex conjugation. For classical dynamics, the time-dependent equations of motion read

$$\mathbf{M}(\mathbf{p}_M) \partial_t^2 \mathbf{y}(t) = \mathbf{K}(\mathbf{p}_K, t) \mathbf{y}(t). \quad (6)$$

The corresponding generalized instantaneous eigenvalue problem is given by

$$\lambda_n(t) \mathbf{M}(\mathbf{p}_M) \mathbf{n}(t) = \mathbf{K}(\mathbf{p}_K, t) \mathbf{n}(t), \quad (7)$$

where $\lambda_n(t) = \omega_n^2(t)$ is the frequency of oscillation squared. The eigenvectors are mass-orthonormal, i.e., $\langle \mathbf{n} | \mathbf{M} | \mathbf{m} \rangle = \delta_{nm}$. If the system is initialized as $\mathbf{y}(0) = \mathbf{n}(0)$ and evolved slow enough, then the solution is well described by [42, 88]

$$\mathbf{y}(t) \approx \sqrt{\frac{\omega_n(0)}{\omega_n(t)}} e^{-i\Omega_n(t)} e^{-i\gamma_n(t)} \mathbf{n}(t), \quad (8)$$

where

$$\Omega(t) = \int_0^t \omega_n(t') dt', \quad (9)$$

and the classical geometric phase reads

$$\gamma_n(t) = \text{Im} \int_0^t \langle \mathbf{n}(t') | \mathbf{M}(\mathbf{p}_M) | \partial_t \mathbf{n}(t') \rangle dt'. \quad (10)$$

A detailed discussion on the differences between quantum and classical adiabatic evolution and an analysis under which respective conditions the adiabatic approximation is valid, can be found in [88].

We assume that the mass and in particular the stiffness matrix are defined over the complex field to cover, e.g., Bloch systems, as discussed in Section 3.5. This implies that the state vector \mathbf{y} can be complex. Real-valued systems can, however, also have a non-trivial Berry phase [88, 89]. Here, the Berry phase encodes the information of whether or not the parallel transported eigenstate reaches the opposite side of the real N -unit sphere or returns to its initial position after a closed loop evolution.

In what follows, we will constrain ourselves to the classical case and note that the quantum Berry phase θ_n is a special case of the classical Berry phase γ_n by choosing $\mathbf{M}(\mathbf{p}_M) := \mathbb{1}$ and $\mathbf{H}(\mathbf{p}_H, t) := \mathbf{K}(\mathbf{p}_K, t)$.

The Berry phase is quantized to 0 or π modulo 2π and acts as a topological invariant in the presence of protecting symmetries [8, 5]. Relaxing those symmetries dequantizes the Berry phase and allows us to compute derivatives [78]. In case of a real-valued system, the Berry phase is protected by the absence of imaginary (self-) couplings. Therefore, differentiability for such a system requires a complex parametrization that can interpolate the two real systems with Berry phases 0 or π .

The contribution of this article is to derive the adjoint method to efficiently compute this parameter derivative $d\gamma_n(t)/d\mathbf{p}_X$. Furthermore, the gradient is exact within the numerical discretization error of the forward problem. This allows us to systematically steer a system through topological phase transition following updates of the form $\mathbf{p}_X \rightarrow \mathbf{p}_X - \alpha d\gamma_n^c/d\mathbf{p}_X$, where α is some optimal step length. Furthermore, the gradient informs us about the robustness of geometric phase devices beyond symmetric perturbation.

3 Adjoint method for geometric phase derivatives

To compute the gradient, we will employ an approximate expression of the Berry phase on the discretized interval $t \in [0, t_I]$ with discrete time points $\{t_i\}_{i=0}^I$ [5]:

$$\begin{aligned} \gamma_n[\mathbf{n}(t_0), \dots, \mathbf{n}(t_I), \mathbf{p}_M] \\ \approx \sum_{i=0}^{I-1} \text{Im} \ln \langle \mathbf{n}(t_i) | \mathbf{M}(\mathbf{p}_M) | \mathbf{n}(t_{i+1}) \rangle, \end{aligned} \quad (11)$$

where, in the interest of the following derivation, we made the eigenvector and parameter dependence of the Berry phase explicit. In the limit where $I \rightarrow \infty$ the above expression converges to the exact Berry phase in Equation (10). We further assume that the loop is closed, i.e. $\mathbf{n}(t_0) = \mathbf{n}(t_I)$, which implies that the Berry phase is gauge invariant, as each eigenvector appears once as a bra and once as a ket. The complex conjugation therefore cancels any phase change in the individual eigenvectors [5]. Consequently, the gradient derived from it also inherits gauge invariance. Equation (11) proves to be the simplest and most practical for our intended purposes. Notably, any

standard eigenvalue solver can be used to determine the eigenstates along the trajectory without necessitating special consideration for relative phase handling. Additionally, this approach possesses the advantage of emulating exact adiabatic evolution even with sparsely sampled time points, which, in our experience, is computationally more efficient than direct adiabatic integration of the time-dependent problem.

Note that equation (11) covers also the case of a non-cyclic Berry phase where the loop is closed along any geodesic that connects $\mathbf{n}(t_0)$ and $\mathbf{n}(t_{I-1})$ [90, 91, 92].

We simplify the notation by introducing $\mathbf{p} := [\mathbf{p}_M, \mathbf{p}_K] \in \mathbb{R}^{N_p}$ and defining $\mathbf{M} := \mathbf{M}(\mathbf{p})$ for the time-dependent mass matrix, $\mathbf{K}_i := \mathbf{K}(\mathbf{p}, t_i)$ for the stiffness matrix, $\lambda_i := \lambda_n(t_i)$ for the instantaneous eigenvalues, and $\mathbf{n}_i := \mathbf{n}(t_i)$ for the eigenvectors.

3.1 From constrained to unconstrained

In practice, the Berry phase of the system will be optimized to some target value $\gamma^{tar.}$, i.e. we minimize an objective function of the form $J = 1/2 \|\gamma_n - \gamma^{tar.}\|^2$. Chain rule implies that $dJ/d\mathbf{p} = \partial J / \partial \gamma_n d\gamma_n / d\mathbf{p} = (\gamma_n - \gamma^{tar.}) d\gamma_n / d\mathbf{p}$. To simplify the notation of the following gradient derivation we cast the optimization problem in terms of minimizing γ_n rather than J .

Direct computation of $d\gamma_n^c / d\mathbf{p} = d\gamma_n^c / d\mathbf{n}_i \partial \mathbf{n}_i / \partial \mathbf{p}$ entails evaluating $\partial \mathbf{n}_i / \partial \mathbf{p}$. However, computing and storing the $\mathbb{C}^{N \times N_p}$ matrix $\partial \mathbf{n}_i / \partial \mathbf{p}$ becomes impractical when \mathbf{n} and \mathbf{p} are high-dimensional. The adjoint procedure presents a solution to eliminate the need for $\partial \mathbf{n}_i / \partial \mathbf{p}$ in gradient computation.

Following the developments in [82] and [81], we address the constrained optimization problem:

$$\begin{aligned} \min_{\mathbf{n}_0, \dots, \mathbf{n}_I, \mathbf{p}} \quad & \gamma_n[\mathbf{n}_0, \dots, \mathbf{n}_I, \mathbf{p}] \quad \text{s.t.} \\ & (\mathbf{K}_i - \lambda_i \mathbf{M}) \mathbf{n}_i = 0, \\ & 1 - \langle \mathbf{n}_i | \mathbf{M} | \mathbf{n}_i \rangle = 0 \quad i = 1, \dots, I, \end{aligned} \quad (12)$$

The first I constraints ensure that the pairs $(\lambda_i, \mathbf{n}_i)$ are solutions to the eigenvalue problem (7). The subsequent set of I constraints enforce that the eigenvectors lie on the mass-induced unit sphere, ensuring well-posedness of the system of

equations. We assume that a unique solution (up to a phase) exists for the eigenvalue problem, denoting it as $(\lambda_i, \mathbf{n}_i) = (\lambda_i(\mathbf{p}), \mathbf{n}_i(\mathbf{p}))$ for a particular \mathbf{p} . Further, we assume differentiability of \mathbf{K}_i and \mathbf{M} with respect to \mathbf{p} .

The transformation of the constrained optimization problem into an unconstrained one is achieved through the concept of Lagrange multipliers. In the realm of PDE-constrained optimization, the Lagrange multipliers correspond to adjoint variables, as will become evident. The Lagrangian takes the form

$$\begin{aligned} \mathcal{L}[\mathbf{n}_0, \dots, \mathbf{n}_I, \lambda_0, \dots, \lambda_I, \mathbf{p}, \mathbf{u}_0, \dots, \mathbf{u}_I, v_0, \dots, v_I] = & \\ & \gamma_n[\mathbf{n}_0, \dots, \mathbf{n}_I, \mathbf{p}] \\ & + \sum_{i=0}^I \langle \mathbf{u}_i | \mathbf{K}_i - \lambda_i \mathbf{M} | \mathbf{n}_i \rangle \\ & + \sum_{i=0}^I \frac{1}{2} v_i^* \left(1 - \langle \mathbf{n}_i | \mathbf{M} | \mathbf{n}_i \rangle \right), \end{aligned} \quad (13)$$

where $\mathbf{u}_i \in \mathbb{C}^n$ and $v_i \in \mathbb{C}$ represent the adjoint variables. The Lagrangian can be evaluated for any $(\lambda_i, \mathbf{n}_i)$. Selecting $(\lambda_i, \mathbf{n}_i)$ to be a solution of the eigenvalue problem, i.e., $(\lambda_i, \mathbf{n}_i) = (\lambda_i(\mathbf{p}), \mathbf{n}_i(\mathbf{p}))$, renders the sum in the equation above equal to 0. We denote the Lagrangian evaluated for this particular choice of \mathbf{p} as $\mathcal{L}|_{\mathbf{p}}$ and similarly the geometric phase as $\gamma_n|_{\mathbf{p}}$. We find that

$$\mathcal{L}|_{\mathbf{p}} = \gamma_n|_{\mathbf{p}} + 0 = \gamma_n|_{\mathbf{p}}. \quad (14)$$

Consequently, taking the design parameter derivative at the points $(\mathbf{n}_i, \lambda_i) = (\mathbf{n}_i(\mathbf{p}), \lambda_i(\mathbf{p}))$, we obtain

$$\frac{d\gamma_n|_{\mathbf{p}}}{dp_m} = \sum_{i=0}^I \partial_{\mathbf{n}_i} \mathcal{L}|_{\mathbf{p}} \partial_{p_m} \mathbf{n}_i + \partial_{p_m} \mathcal{L}|_{\mathbf{p}} + \partial_{p_m} \gamma_n|_{\mathbf{p}}, \quad (15)$$

where

$$\partial_{p_m} \gamma_n|_{\mathbf{p}} = \sum_{i=1}^I \text{Im} \ln \langle \mathbf{n}_i(\mathbf{p}) | \partial_{p_m} \mathbf{M} | \mathbf{n}_{i+1}(\mathbf{p}) \rangle. \quad (16)$$

3.2 The adjoint problem and the gradient

Among all possible choices for $\mathbf{u}_0, \dots, \mathbf{u}_I$ and v_0, \dots, v_I , let us denote $\mathbf{u}_0(\mathbf{p}), \dots, \mathbf{u}_I(\mathbf{p})$ and $v_0(\mathbf{p}), \dots, v_I(\mathbf{p})$ as the adjoint variables that satisfy $\partial\mathcal{L}|_{\partial\mathbf{p}}/\partial\mathbf{n}_i = 0$. When such adjoint variables exist, the first term in the above sum becomes zero. The equations emerging from equation (13) when requiring that $\partial\mathcal{L}|_{\partial\mathbf{p}}/\partial\mathbf{n}_i = 0$ are referred to as the adjoint problem, given by

$$\begin{bmatrix} \mathbf{K}_i - \lambda_i \mathbf{M} & -\mathbf{M}\mathbf{n}_i(\mathbf{p}) \\ -\mathbf{n}_i^\dagger(\mathbf{p})\mathbf{M} & 0 \end{bmatrix} \begin{bmatrix} \mathbf{u}_i(\mathbf{p}) \\ v_i(\mathbf{p}) \end{bmatrix} = \begin{bmatrix} -(\partial_{\mathbf{n}_i}\gamma_n)^\dagger \\ 0 \end{bmatrix}. \quad (17)$$

The superscript \dagger denotes conjugate transposition. The right-hand side is the adjoint source and can be obtained analytically as demonstrated below. The matrix on the left-hand side is proven to be invertible in [81]. Hence, $\mathbf{u}_0(\mathbf{p}), \dots, \mathbf{u}_I(\mathbf{p})$ and $v_0(\mathbf{p}), \dots, v_I(\mathbf{p})$ exist and are unique. Therefore, with the choice of $\mathbf{u}_0 = \mathbf{u}_0(\mathbf{p}), \dots, \mathbf{u}_I = \mathbf{u}_I(\mathbf{p})$ and $v_0 = v_0(\mathbf{p}), \dots, v_I = v_I(\mathbf{p})$, we have $\partial\mathcal{L}/\partial\mathbf{n}_i = 0$, and equation (15) reduces to

$$\begin{aligned} \frac{d\gamma_n|_{\mathbf{p}}}{dp_m} &= \partial_{p_m}\mathcal{L}|_{\mathbf{p}} + \partial_{p_m}\gamma_n|_{\mathbf{p}} \\ &= \sum_{i=0}^I \left\langle \mathbf{u}_i(\mathbf{p}) | \partial_{p_m}\mathbf{K}_i - \lambda_i \partial_{p_m}\mathbf{M} | \mathbf{n}_i(\mathbf{p}) \right\rangle \\ &+ \sum_{i=0}^I \frac{1}{2} v_i^*(\mathbf{p}) \left(1 - \langle \mathbf{n}_i(\mathbf{p}) | \partial_{p_m}\mathbf{M} | \mathbf{n}_i(\mathbf{p}) \rangle \right) \\ &+ \sum_{i=0}^I \text{Im} \ln \langle \mathbf{n}_i(\mathbf{p}) | \partial_{p_m}\mathbf{M} | \mathbf{n}_i(\mathbf{p}) \rangle, \quad (18) \end{aligned}$$

where the design parameter derivative of the stiffness and mass matrices can often be obtained analytically. Note that the Berry phase and hence its gradient only exist for parameters where the eigenvalue gap to other eigenstates does not vanish. Otherwise, the Berry phase is not well-defined. It remains to compute the adjoint source.

3.3 The adjoint source

To avoid considerations about the analyticity of the complex eigenstates involved, we treat the real

and imaginary parts as separate components of a vector for the differentiation of the Berry phase. The augmented state vectors are defined as

$$\hat{\mathbf{n}}_i = \begin{bmatrix} \text{Re } \mathbf{n}_i \\ \text{Im } \mathbf{n}_i \end{bmatrix}^T \in \mathbb{R}^{2N}, \quad (19)$$

and the augmented symmetric mass matrix

$$\hat{\mathbf{M}} = \begin{bmatrix} \mathbf{M} & 0 \\ 0 & \mathbf{M} \end{bmatrix}. \quad (20)$$

We further define

$$\hat{\mathbf{Q}} = \begin{bmatrix} \mathbf{0}_{N \times N} & \mathbf{1}_{N \times N} \\ -\mathbf{1}_{N \times N} & \mathbf{0}_{N \times N} \end{bmatrix} \in \mathbb{R}^{2N \times 2N}. \quad (21)$$

In this augmented space, the original mass induced inner product, $\langle \mathbf{n} | \mathbf{M} | \mathbf{m} \rangle$, can be computed as $\langle \mathbf{n} | \mathbf{M} | \mathbf{m} \rangle = \langle \hat{\mathbf{n}} | \hat{\mathbf{M}} | \hat{\mathbf{m}} \rangle + i \langle \hat{\mathbf{n}} | \hat{\mathbf{Q}}\hat{\mathbf{M}} | \hat{\mathbf{m}} \rangle$. We denote the local phase mismatches or local Berry phases, where \mathbf{n}_i contributes, as

$$\begin{aligned} \gamma_n^{i-1} &= \text{Im} \ln \langle \mathbf{n}_{i-1} | \mathbf{M} | \mathbf{n}_i \rangle \\ &= \text{Im} \ln \left(\langle \hat{\mathbf{n}}_{i-1} | \hat{\mathbf{M}} | \hat{\mathbf{n}}_i \rangle + i \langle \hat{\mathbf{n}}_{i-1} | \hat{\mathbf{Q}}\hat{\mathbf{M}} | \hat{\mathbf{n}}_i \rangle \right), \quad (22) \end{aligned}$$

and

$$\begin{aligned} \gamma_n^i &= \text{Im} \ln \langle \mathbf{n}_i | \mathbf{M} | \mathbf{n}_{i+1} \rangle \\ &= \text{Im} \ln \left(\langle \hat{\mathbf{n}}_i | \hat{\mathbf{M}} | \hat{\mathbf{n}}_{i+1} \rangle + i \langle \hat{\mathbf{n}}_i | \hat{\mathbf{Q}}\hat{\mathbf{M}} | \hat{\mathbf{n}}_{i+1} \rangle \right), \quad (23) \end{aligned}$$

where the order in the inner product is swapped for γ_n^{i-1} . Since \mathbf{n}_i only appears in these two terms of the Berry phase, we have

$$\partial_{\hat{\mathbf{n}}_i}\gamma_n = \partial_{\hat{\mathbf{n}}_i}\gamma_n^{i-1} + \partial_{\hat{\mathbf{n}}_i}\gamma_n^i \in \mathbb{R}^{1 \times 2N}. \quad (24)$$

Using $\partial_x \ln x = 1/x$, we can compute the partial derivatives of the two contributions in the augmented space as

$$\begin{aligned} \partial_{\hat{\mathbf{n}}_i}\gamma_n^{i-1} &= \frac{1}{\langle \hat{\mathbf{n}}_i | \hat{\mathbf{M}} | \hat{\mathbf{n}}_{i-1} \rangle^2 + \langle \hat{\mathbf{n}}_i | \hat{\mathbf{Q}}\hat{\mathbf{M}} | \hat{\mathbf{n}}_{i-1} \rangle^2} \\ &\left(\langle \hat{\mathbf{n}}_i | \hat{\mathbf{M}} | \hat{\mathbf{n}}_{i-1} \rangle \hat{\mathbf{n}}_{i-1}^T \hat{\mathbf{Q}}\hat{\mathbf{M}} - \langle \hat{\mathbf{n}}_i | \hat{\mathbf{Q}}\hat{\mathbf{M}} | \hat{\mathbf{n}}_{i-1} \rangle \hat{\mathbf{n}}_{i-1}^T \hat{\mathbf{M}} \right) \quad (25) \end{aligned}$$

and

$$\partial_{\hat{\mathbf{n}}_i} \gamma_n^i = \frac{1}{\langle \hat{\mathbf{n}}_i | \hat{\mathbf{M}} | \hat{\mathbf{n}}_{i+1} \rangle^2 + \langle \hat{\mathbf{n}}_i | \hat{\mathbf{Q}} \hat{\mathbf{M}} | \hat{\mathbf{n}}_{i+1} \rangle^2} \left(\langle \hat{\mathbf{n}}_i | \hat{\mathbf{M}} | \hat{\mathbf{n}}_{i+1} \rangle \hat{\mathbf{n}}_{i+1}^T \hat{\mathbf{M}} \hat{\mathbf{Q}}^T - \langle \hat{\mathbf{n}}_i | \hat{\mathbf{Q}} \hat{\mathbf{M}} | \hat{\mathbf{n}}_{i+1} \rangle \hat{\mathbf{n}}_{i+1}^T \hat{\mathbf{M}} \right). \quad (26)$$

With these definitions, the adjoint source at time $t = t_i$ can be found as

$$\partial_{\hat{\mathbf{n}}_i} \gamma_n |_{\mathbf{p}} = \partial_{\hat{\mathbf{n}}_i} \gamma_n [1 : N] + i \partial_{\hat{\mathbf{n}}_i} \gamma_n [N + 1 : 2N] \in \mathbb{C}^{1 \times N}. \quad (27)$$

3.4 The algorithm

In summary, to compute the design parameter gradient, we follow Algorithm 3.4. We emphasize that

Algorithm 1 Berry phase gradient

1. Solve $\lambda_i \mathbf{M}(t_i) \mathbf{n}_i = \mathbf{K}(t_i) \mathbf{n}_i$ for $\{t_i\}_{i=0, \dots, I}$ to obtain $\{\mathbf{n}_i\}_{i=0, \dots, I}$, $\{\lambda_i\}_{i=0, \dots, I}$
 2. Compute the adjoint sources $\partial_{\hat{\mathbf{n}}_i} \gamma_n |_{\mathbf{p}}$ for $\{t_i\}_{i=0, \dots, I}$
 3. Solve adjoint problem (17) to obtain adjoint variables $\{\mathbf{u}_i(\mathbf{p})\}_{i=0, \dots, I}$ and $\{v_i(\mathbf{p})\}_{i=0, \dots, I}$
 4. Evaluate $\partial_{p_m} \mathbf{M}$ and $\partial_{p_m} \mathbf{K}_i$
 5. Compute the design parameter gradient as in equation (18) for all model parameters p_0, \dots, p_{N_p}
-

if $\partial_{p_m} \mathbf{K}_i$ and $\partial_{p_m} \mathbf{M}$ can be obtained analytically, they do not need to be explicitly constructed. Instead, equation (18) can be efficiently implemented as a vector-matrix product and steps 4 and 5 of Algorithm 3.4 can be merged. This approach significantly reduces computational overhead and memory requirements.

In the context of optimizing the geometric phase, it is necessary to maintain a gap between adjacent eigenvalue levels. Remarkably, within this framework, the design parameter gradient of the gap can be derived from the gradient of the eigenvalues, which is readily computed as [81]

$$\frac{d\lambda_i}{dp_m} = \left\langle \mathbf{n}_i(\mathbf{p}) \left| \partial_{p_m} \mathbf{K}_i - \lambda_i \partial_{p_m} \mathbf{M} \right| \mathbf{n}_i(p) \right\rangle. \quad (28)$$

3.5 Application to a continuous 1D elastic topological metamaterial: Hockey-Stick-Test

In this section, we utilize the adjoint method to calculate the gradient of the Berry phase of a continuous elastic metamaterial rod. To validate the correctness of the gradient, we subject it to a Hockey-Stick-Test [93]. We consider a one-dimensional elastic crystal, which, when inversion symmetry is present, can exhibit a topological phase [94, 95]. This elastic rod is aligned along the x -axis and has a unit cell of width W , with elastic modulus $E(x + W) = E(x)$ and density $\rho(x + W) = \rho(x)$. The rod satisfies the linear elastic wave equation

$$\rho(x) \partial_t^2 y(t, x) = \partial_x \left[E(x) \partial_x y(t, x) \right], \quad (29)$$

where y represents the transverse or horizontal displacement along the longitudinal direction. The generalized eigenvalue problem reads

$$\lambda_n(k) \rho(x) n(x, k) = \partial_x E(x) \partial_x n(x, k). \quad (30)$$

The Bloch theorem [96, 5] guarantees that the eigenvectors are given by $y_n(x, k) = \exp(-ikx/W) n(x, k)$, where k is the Bloch wavenumber. Here, $n(x, k)$ corresponds to the Bloch wave functions, exhibiting the same periodicity as the lattice, i.e., $n(x + W, k) = n(x, k)$. The corresponding instantaneous frequency, $\omega_n(k)$, is given by the square root of the eigenvalue $\lambda_n(k)$. Plotting $\lambda_n(k)$ or $\omega_n(k)$ for each n as a function of k yields the band structure, as shown in Figure 1(b). The eigenvalues and Bloch wave functions are determined through the generalized Bloch eigenvalue problem

$$\begin{aligned} \lambda_n(k) \rho(x) n(x, k) &= e^{ikx/W} \left[\partial_x E(x) \partial_x \right] e^{-ikx/W} n(x, k) \\ &= \left[\partial_x E(x) \partial_x + ik \left(2E(x) \partial_x + \partial_x E(x) \right) - E(x) k^2 \right] n(x, k). \end{aligned} \quad (31)$$

Now, we employ the spectral-element method [83, 97] to discretize this eigenvalue problem. The spectral-element method is a finite-element-like discretization scheme that produces diagonal mass

matrices and has been recognized for its effectiveness in solving wave problems. We define the $N \times N$ assembly stiffness matrices obtained by discretizing the above operators as $\partial_x E(x) \partial_x \rightarrow \mathbf{K}_a$, $2E(x) \partial_x + \partial_x E(x) \rightarrow \mathbf{K}_b$, and $E(x) \rightarrow \mathbf{K}_c$. The discretized Bloch stiffness matrix is given by

$$\mathbf{K}(\mathbf{p}, k) = \frac{1}{\rho} (\mathbf{K}_a(\mathbf{p}) + ik\mathbf{K}_b(\mathbf{p}) - k^2\mathbf{K}_c(\mathbf{p})). \quad (32)$$

For simplicity, we assume a constant value for the density and absorb it into the stiffness matrix. However, the method can be straightforwardly generalized to accommodate arbitrary density profiles. Finally, discretizing $n \rightarrow \mathbf{n}$ we obtain the generalized eigenvalue problem (7) for a constant mass matrix and where the Bloch wavenumber plays the role of time.

It can be shown that the eigenvalues are periodic in k -space, meaning that $\lambda_n(k + 2\pi/W) = \lambda_n(k)$ [96]. From now on, we will work in a periodic gauge [5], meaning that we have $\mathbf{n}(k + 2\pi/W) = \mathbf{n}(k)$ (not just up to a phase). This implies that we can confine ourselves to the Brillouin Zone (BZ), which ranges from $-\pi/W$ to π/W . The periodic gauge relates Bloch functions as follows: $\exp(-i(k + 2\pi)x/W)\mathbf{n}(k + 2\pi) = \exp(-ikx/W)\mathbf{n}(k)$, which implies that $\mathbf{n}(k) = \exp(-ikx/W)\mathbf{n}(k + 2\pi)$. Let us divide the BZ into discrete intervals of Bloch wavenumber $k_0 = -\pi/W, \dots, k_I = \pi/W$. While we opt for equidistantly distributed k -points in this analysis, this choice is not mandatory. The single-band Berry phase, known as the Zak phase in this context, can be computed as

$$\gamma_n = \sum_{i=0}^{N-1} \text{Im} \ln \langle \mathbf{n}(k_i) | \mathbf{n}(k_{i+1}) \rangle + \text{Im} \ln \langle \mathbf{n}(k_I) | e^{-i2\pi x/W} | \mathbf{n}(k_0) \rangle. \quad (33)$$

The additional phase factor, $\exp(-ikx/W)$, that emerges is a peculiar characteristic of the Zak phase [98, 5]. In systems with, e.g., inversion symmetry, the Zak phase is quantized to 0 or π (modulo 2π) [98, 95, 8]. However, in systems lacking symmetries, the Berry phase can assume any value, and it exhibits almost everywhere differentiability [78]. If discretized, the Zak phase may act as a topological invariant, which, through the

Bulk-Edge-Correspondence, predicts the existence or absence of topological surface modes.

We now turn our attention to computing the gradient of the Zak phase for the first ($n = 0$) band with respect to all model parameters, denoted as $d\gamma_0/d\mathbf{p}$. In the specific example presented here, we employed $N = 200$ grid points, and an equal number of model parameters, i.e., $N_p = N$. The gradient obtained from the adjoint method is represented by $\mathbf{g}_{adj}(\mathbf{p}) = d\gamma_0/d\mathbf{p} \in \mathbb{R}^{N_p}$. We evaluate this gradient for the metamaterial rod. The rod's elastic modulus profile $E(x)$ is depicted Figure 1(a) and the density is set to a constant value of $\rho = 2704 \text{ kg/m}^3$. In this configuration, we find that $\gamma_0(\mathbf{p}) = 0$, indicating a topologically trivial phase. The Zak phase is quantized, a result of the inversion symmetry. In Figure 1(a), the gradient distribution throughout the unit cell is depicted on top of the elastic modulus profile. The gradient informs us that we have to break the inversion symmetry to change the Zak phase.

We aim to compare the gradient derived from the adjoint method, \mathbf{g}_{adj} , with the gradient obtained through first-order finite differentiation, \mathbf{g}_{fd} through a Hockey-Stick test [93]. The latter is determined by perturbing each model parameter individually by a small amount, δp , and subsequently recalculating all the eigenvectors along the path. Specifically, for a perturbation in the m -th model parameter, the perturbed parameter set is $\mathbf{p}_m^{pert} = [p_1, \dots, p_m + \delta p, \dots, p_M]$. The gradient through first-order finite differentiation for each model parameter (here equivalently, for each numerical grid point) is then given by

$$[\mathbf{g}_{fd}(\mathbf{p})]_m = \frac{\gamma_0(\mathbf{p}_m^{pert}) - \gamma_0(\mathbf{p})}{\delta p}. \quad (34)$$

The Hockey-Stick-Test involves successively reducing δp and juxtaposing the gradient from first-order finite differentiation against the adjoint gradient (Figure 1(c)). Given that the adjoint gradient is exact (assuming its correct computation), one anticipates the discrepancy between the two gradients to diminish as δp reduces. However, at a certain threshold of δp , floating point errors start to dominate over a theoretically improved finite differentiation, rendering the gradient from finite differentiation increasingly inaccurate. Consequently, a hockey stick shaped divergence between the numerical and adjoint gradients is

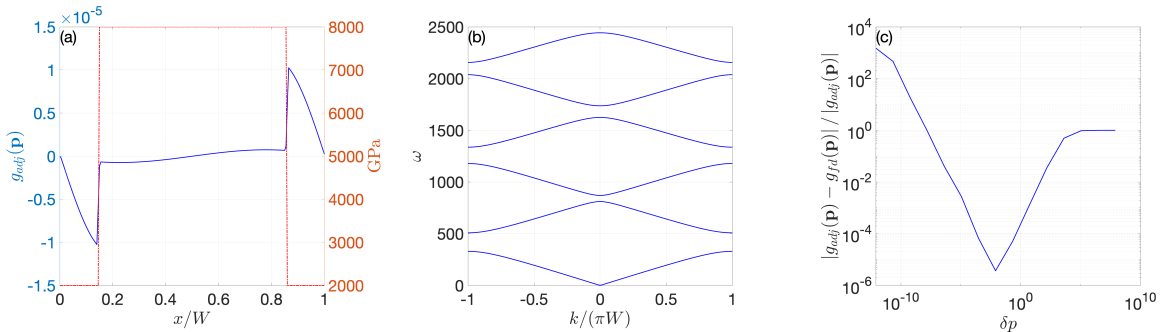


Fig. 1 (a) Elastic modulus profile across the unit cell in red and the gradient of the Berry phase of the 1st band in blue. From the profile, it is evident that altering the Zak phase necessitates breaking its inversion symmetry. (b) Bloch band structure over the Brillouin Zone. (c) Hockey-Stick-Test: The y-axis depicts the relative disparity between the adjoint and first-order finite differentiation gradients across varying design parameter perturbations (x-axis). The distinctive “hockey stick” curvature of the plot robustly underscores the accuracy of the adjoint gradient.

predicted for diminishing values of δp [93]. Figure 1(c) shows that the gradient test indeed behaves as expected.

3.6 Algorithm complexity

For computing a Berry phase with I discrete time or Bloch wavenumber points, the algorithmic complexity of the adjoint method corresponds to the sum of I eigenvalue solver instances plus I adjoint problems. The latter equates to I system of equation solutions. Significantly, this complexity is not influenced by the number of model parameters. On the other hand, O -order finite differentiation necessitates $O \times I$ eigenvalue problem solutions for each model parameter, leading to a complexity proportional to $O \times I \times (N_p + 1)$ eigenvalue solutions. Thus, as N_p , the number of model parameters grows, the adjoint method outperforms finite differentiation. Additionally, in contrast to finite differentiation which suffers from truncation and floating point errors as δp approaches 0, the adjoint method provides an exact gradient within the approximation of the forward discretization.

4 Generalization to Multiband Berry Phases

In this section, we discuss the generalization of the proposed method to the multiband, or non-Abelian Berry phase, which is computed using the Wilson loop approach [99]. For a detailed physical

derivation and the relation to polarization, maximally localized Wannier functions, or topology, we refer to, e.g., [5, 100, 8, 101]. A discussion on the appearance of these quantities in classical mechanics and how they differ from the quantum case can be found in [88].

We consider a set of B isolated bands below a band gap of interest and introduce the overlap matrix as

$$\begin{aligned} \mathbf{U}_{n,m}^{(i,i+1)} &= \langle \mathbf{n}_i | \mathbf{M} | \mathbf{m}_{i+1} \rangle \\ &= \langle \hat{\mathbf{n}}_i | \hat{\mathbf{M}} | \hat{\mathbf{m}}_{i+1} \rangle + i \langle \hat{\mathbf{n}}_i | \hat{\mathbf{Q}}\hat{\mathbf{M}} | \hat{\mathbf{m}}_{i+1} \rangle, \end{aligned} \quad n, m \in B, \quad (35)$$

where we have used the definitions in equations (19)-(21). We assume a closed loop, i.e., $\mathbf{n}_0 = \mathbf{n}_I$, for all bands. The gauge-invariant multiband Berry phase is given by [5]

$$\gamma_{\text{tot}}[\{\{\mathbf{n}_i\}_{i=0}^I\}_{n \in B}, \mathbf{p}] \approx \sum_{i=0}^I \text{Im} \ln \det \mathbf{U}^{(i,i+1)}. \quad (36)$$

Note that the above expression is exact in the limit $I \rightarrow \infty$ [8, 5]. While this would typically require handling points or intervals of degeneracies below the gap, we now argue that this is not needed in practice.

First note that, in the case where all the bands below the band gap of interest are themselves gapped, the multiband Berry phase decomposes into the sum of the Berry phases of the individual

bands, i.e.

$$\gamma_{\text{tot}}[\{\{\mathbf{n}_i\}_{i=0}^I\}_{n \in B}, \mathbf{p}] = \sum_{n \in B} \gamma_n. \quad (37)$$

Furthermore, the multiband Berry phase is a smooth function of the system parameters as long as the gap of interest stays open. Thus, an infinitesimal symmetry-breaking perturbation that lifts degeneracies below the gap will only cause a smooth change in the multiband Berry phase, even if individual Berry phases change abruptly.

Thus, we can always introduce small perturbations to lift all degeneracies without closing the gap of interest, as an infinitesimal perturbation is enough to open a gap but cannot close a finite one. In practice, this can be done by adding a small random Hermitian perturbation, $\delta\mathbf{p}$, to the Hamiltonian or stiffness matrix to break all symmetries in the system. Then the gradient of the multiband Berry phase can readily be computed with the presented method above as

$$\frac{d\gamma_{\text{tot}}|_{\mathbf{p}+\delta\mathbf{p}}}{dp_m} = \sum_{n \in B} \frac{d\gamma_n|_{\mathbf{p}+\delta\mathbf{p}}}{dp_m}. \quad (38)$$

If $\delta\mathbf{p}$ is sufficiently small we approximately have that

$$\frac{d\gamma_{\text{tot}}|_{\mathbf{p}+\delta\mathbf{p}}}{dp_m} \approx \frac{d\gamma_{\text{tot}}|_{\mathbf{p}}}{dp_m}. \quad (39)$$

5 Conclusions

We developed the adjoint method to compute parameter gradients of the Berry phase. The method can be applied to devices based on adiabatic evolution, as well as to metamaterial systems, where the Berry or Zak phase serves as a topological invariant. The approach is effective for both single and multiband Berry phases. Combined with tools like topology optimization, this method enables the systematic design of continuous space-time materials and devices that exploit geometric and topological wave propagation.

Acknowledgements. We wish to thank Frank Schindler, Tena Dubcek, Sebastian Huber, Valerio Peri, Aleksandra Nelson and Tomáš Bzdušek for helpful discussion. Furthermore, C. B. and A. F. acknowledge funding from ETH Zurich. M.S. acknowledges support by ERC grant (Project No.

101040117). Views and opinions expressed are however those of the author(s) only and do not necessarily reflect those of the European Union or the European Research Council Executive Agency. Neither the European Union nor the granting authority can be held responsible for them.

Conflict of interest statement. On behalf of all authors, the corresponding author states that there is no conflict of interest.

Replication of results. Source codes to replicate all the results presented in this article can be found in the Supplementary Material. The code will produce Figure 1.

References

- [1] Michael Victor Berry. Quantal phase factors accompanying adiabatic changes. *Proceedings of the Royal Society of London. A. Mathematical and Physical Sciences*, 392(1802):45–57, 1984.
- [2] K v Klitzing, Gerhard Dorda, and Michael Pepper. New method for high-accuracy determination of the fine-structure constant based on quantized Hall resistance. *Physical review letters*, 45(6):494, 1980.
- [3] David J Thouless, Mahito Kohmoto, M Peter Nightingale, and Marcel den Nijs. Quantized hall conductance in a two-dimensional periodic potential. *Physical review letters*, 49(6):405, 1982.
- [4] Z-H Zhu, G Levy, B Ludbrook, CN Veenstra, JA Rosen, R Comin, D Wong, P Dosanjh, A Ubaldini, P Syers, et al. Rashba spin-splitting control at the surface of the topological insulator Bi₂Se₃. *Physical review letters*, 107(18):186405, 2011.
- [5] David Vanderbilt. *Berry Phases in Electronic Structure Theory: Electric Polarization, Orbital Magnetization and Topological Insulators*. Cambridge University Press, 2018.
- [6] Shinsei Ryu, Andreas P Schnyder, Akira Furusaki, and Andreas WW Ludwig. Topological insulators and superconductors: tenfold way and dimensional hierarchy. *New Journal of Physics*, 12(6):065010, 2010.

- [7] Aris Alexandradinata and B Andrei Bernevig. Berry-phase description of topological crystalline insulators. *Physical Review B*, 93(20):205104, 2016.
- [8] Titus Neupert and Frank Schindler. Topological crystalline insulators. In *Topological Matter*, pages 31–61. Springer, 2018.
- [9] Liang Fu. Topological crystalline insulators. *Phys. Rev. Lett.*, 106:106802, Mar 2011.
- [10] Robert-Jan Slager, Andrej Mesaros, Vladimir Juričić, and Jan Zaanen. The space group classification of topological band-insulators. *Nature Physics*, 9(2):98–102, Feb 2013.
- [11] A Yu Kitaev. Unpaired Majorana fermions in quantum wires. *Physics-uspekhi*, 44(10S):131, 2001.
- [12] Ling Lu, John D Joannopoulos, and Marin Soljačić. Topological photonics. *Nature photonics*, 8(11):821–829, 2014.
- [13] Tomoki Ozawa, Hannah M Price, Alberto Amo, Nathan Goldman, Mohammad Hafezi, Ling Lu, Mikael C Rechtsman, David Schuster, Jonathan Simon, Oded Zilberberg, et al. Topological photonics. *Reviews of Modern Physics*, 91(1):015006, 2019.
- [14] Daria Smirnova, Daniel Leykam, Yidong Chong, and Yuri Kivshar. Nonlinear topological photonics. *Applied Physics Reviews*, 7(2), 2020.
- [15] Jiho Noh, Wladimir A Benalcazar, Sheng Huang, Matthew J Collins, Kevin P Chen, Taylor L Hughes, and Mikael C Rechtsman. Topological protection of photonic mid-gap defect modes. *Nature Photonics*, 12(7):408–415, 2018.
- [16] Mikael C Rechtsman, Julia M Zeuner, Yonatan Plotnik, Yaakov Lumer, Daniel Podolsky, Felix Dreisow, Stefan Nolte, Mordechai Segev, and Alexander Szameit. Photonic Floquet topological insulators. *Nature*, 496(7444):196–200, 2013.
- [17] Jiho Noh, Sheng Huang, Kevin P Chen, and Mikael C Rechtsman. Observation of photonic topological valley Hall edge states. *Physical review letters*, 120(6):063902, 2018.
- [18] Mikael C Rechtsman, Yonatan Plotnik, Julia M Zeuner, Daohong Song, Zhigang Chen, Alexander Szameit, and Mordechai Segev. Topological creation and destruction of edge states in photonic graphene. *Physical review letters*, 111(10):103901, 2013.
- [19] Mohammad-Ali Miri and Andrea Alu. Exceptional points in optics and photonics. *Science*, 363(6422):eaar7709, 2019.
- [20] Xiang Ni, Simon Yves, Alex Krasnok, and Andrea Alù. Topological metamaterials. *Chemical Reviews*, 2023.
- [21] Siying Peng, Nick J Schilder, Xiang Ni, Jorik Van De Groep, Mark L Brongersma, Andrea Alù, Alexander B Khanikaev, Harry A Atwater, Albert Polman, et al. Probing the band structure of topological silicon photonic lattices in the visible spectrum. *Physical review letters*, 122(11):117401, 2019.
- [22] Juan Kang, Ruishan Wei, Qinglong Zhang, and Guoping Dong. Topological Photonic States in Waveguide Arrays. *Advanced Physics Research*, 2(3):2200053, March 2023.
- [23] Xu-Lin Zhang, Feng Yu, Ze-Guo Chen, Zhen-Nan Tian, Qi-Dai Chen, Hong-Bo Sun, and Guancong Ma. Non-Abelian braiding on photonic chips. *Nat. Photon.*, 16(5):390–395, May 2022.
- [24] Gabriel Cáceres-Aravena, Bastián Real, Diego Guzmán-Silva, Alberto Amo, Luis E. F. Foa Torres, and Rodrigo A. Vicencio. Experimental observation of edge states in SSH-Stub photonic lattices. *Phys. Rev. Research*, 4(1):013185, March 2022.
- [25] Mohit Kumar and Fabio Semperlotti. On the role of geometric phase in the dynamics of elastic waveguides. *Philosophical Transactions A*, 382(2279):20230357, 2024.
- [26] Sebastian D Huber. Topological mechanics. *Nature Physics*, 12(7):621–623, 2016.
- [27] Roman Süssstrunk and Sebastian D Huber. Classification of topological phonons in linear mechanical metamaterials. *Proceedings of the National Academy of Sciences*, 113(33):E4767–E4775, 2016.
- [28] Ting-Wei Liu and Fabio Semperlotti. Tunable acoustic valley-hall edge states in reconfigurable phononic elastic waveguides. *Physical Review Applied*, 9(1):014001, 2018.
- [29] Pai Wang, Ling Lu, and Katia Bertoldi. Topological phononic crystals with one-way elastic edge waves. *Physical review letters*, 115(10):104302, 2015.

- [30] Emanuele Riva, Matheus IN Rosa, and Massimo Ruzzene. Edge states and topological pumping in stiffness-modulated elastic plates. *Physical Review B*, 101(9):094307, 2020.
- [31] Yizhou Liu, Yong Xu, Shou-Cheng Zhang, and Wenhui Duan. Model for topological phononics and phonon diode. *Physical Review B*, 96(6):064106, 2017.
- [32] Emanuele Riva, Gianmaria Castaldini, and Francesco Braghin. Adiabatic edge-to-edge transformations in time-modulated elastic lattices and non-Hermitian shortcuts. *New J. Phys.*, 23(9):093008, September 2021.
- [33] Mou Yan, Jiuyang Lu, Feng Li, Weiyin Deng, Xueqin Huang, Jiahong Ma, and Zhengyou Liu. On-chip valley topological materials for elastic wave manipulation. *Nature Materials*, 17(11):993–998, 2018.
- [34] Javier Vila, Raj Kumar Pal, and Massimo Ruzzene. Observation of topological valley modes in an elastic hexagonal lattice. *Physical Review B*, 96(13):134307, 2017.
- [35] CL Kane and TC Lubensky. Topological boundary modes in isostatic lattices. *Nature Physics*, 10(1):39–45, 2014.
- [36] Emil Prodan and Camelia Prodan. Topological phonon modes and their role in dynamic instability of microtubules. *Physical review letters*, 103(24):248101, 2009.
- [37] Nina Berg, Kira Joel, Miriam Koolyk, and Emil Prodan. Topological phonon modes in filamentary structures. *Physical Review E*, 83(2):021913, 2011.
- [38] TC Lubensky, CL Kane, Xiaoming Mao, Anton Souslov, and Kai Sun. Phonons and elasticity in critically coordinated lattices. *Reports on Progress in Physics*, 78(7):073901, 2015.
- [39] Kathryn H. Matlack, Marc Serra-Garcia, Antonio Palermo, Sebastian D. Huber, and Chiara Daraio. Designing perturbative metamaterials from discrete models. *Nature Materials*, 2018.
- [40] Marc Serra-Garcia, Valerio Peri, Roman Süssstrunk, Osama R. Bilal, Tom Larsen, Luis Guillermo Villanueva, and Sebastian D. Huber. Observation of a phononic quadrupole topological insulator. *Nature*, 555:342 EP –, 01 2018.
- [41] Valerio Peri, Zhi-Da Song, Marc Serra-Garcia, Pascal Engeler, Raquel Queiroz, Xueqin Huang, Weiyin Deng, Zhengyou Liu, B Andrei Bernevig, and Sebastian D Huber. Experimental characterization of fragile topology in an acoustic metamaterial. *Science*, 367(6479):797–800, 2020.
- [42] H Nassar, H Chen, AN Norris, and GL Huang. Quantization of band tilting in modulated phononic crystals. *Physical Review B*, 97(1):014305, 2018.
- [43] S. Hossein Mousavi, Alexander B. Khanikaev, and Zheng Wang. Topologically protected elastic waves in phononic metamaterials. *Nature Communications*, 6:8682 EP –, Nov 2015. Article.
- [44] Ting-Wei Liu and Fabio Semperlotti. Classical analogue to the Kitaev model and majoranalike topological bound states. *Physical Review Applied*, 20(1):014019, 2023.
- [45] Yiwei Xia, Emanuele Riva, Matheus IN Rosa, Gabriele Cazzulani, Alper Erturk, Francesco Braghin, and Massimo Ruzzene. Experimental observation of temporal pumping in electromechanical waveguides. *Physical Review Letters*, 126(9):095501, 2021.
- [46] Paolo Zanardi and Mario Rasetti. Holonomic quantum computation. *Physics Letters A*, 264(2-3):94–99, 1999.
- [47] Paolo Solinas, Paolo Zanardi, and Nino Zanghì. Robustness of non-Abelian holonomic quantum gates against parametric noise. *Physical Review A*, 70(4):042316, 2004.
- [48] Shi-Liang Zhu and Paolo Zanardi. Geometric quantum gates that are robust against stochastic control errors. *Physical Review A*, 72(2):020301, 2005.
- [49] Ivette Fuentes-Guridi, Florian Girelli, and E Livine. Holonomic quantum computation in the presence of decoherence. *Physical review letters*, 94(2):020503, 2005.
- [50] Chandroth Pannian Jisha, Stefan Nolte, and Alessandro Alberucci. Geometric phase in optics: from wavefront manipulation to waveguiding. *Laser & Photonics Reviews*, 15(10):2100003, 2021.
- [51] Qian Lin and Shanhui Fan. Light guiding by effective gauge field for photons. *Physical*

- Review X*, 4(3):031031, 2014.
- [52] Dingyu Xu, Hua Yang, Wenhao Xu, Wenshuai Zhang, Kuiming Zeng, and Hailu Luo. Inverse design of Pancharatnam–Berry phase metasurfaces for all-optical image edge detection. *Applied Physics Letters*, 120(24):241101, June 2022.
- [53] Chandroth P Jisha, Stree Vithya Arumugam, Lorenzo Marrucci, Stefan Nolte, and Alessandro Alberucci. Waveguiding driven by the Pancharatnam–Berry phase. *Physical Review A*, 107(1):013523, 2023.
- [54] Michael J Escuti, Jihwan Kim, and Michael W Kudenov. Controlling light with geometric-phase holograms. *Optics and Photonics News*, 27(2):22–29, 2016.
- [55] Andrew Forbes. Structured light: tailored for purpose. *Optics and Photonics News*, 31(6):24–31, 2020.
- [56] Roel Snieder, Christoph Sens-Schönfelder, Elmer Ruigrok, and Katsuhiko Shiomi. Seismic shear waves as foucault pendulum. *Geophysical Research Letters*, 43(6):2576–2581, 2016.
- [57] Jérémie Boulanger, Nicolas Le Bihan, Stefan Catheline, and Vincent Rossetto. Observation of a non-adiabatic geometric phase for elastic waves. *Annals of Physics*, 327(3):952–958, 2012.
- [58] Erik Sjöqvist. Geometric phases in quantum information. *International Journal of Quantum Chemistry*, 115(19):1311–1326, 2015.
- [59] Sun Yin and DM Tong. Geometric phase of a quantum dot system in nonunitary evolution. *Physical Review A*, 79(4):044303, 2009.
- [60] Stefano Cusumano, Antonella De Pasquale, and Vittorio Giovannetti. Geometric phase through spatial potential engineering. *Physical Review Letters*, 124(19):190401, 2020.
- [61] Luqing Qiu, Hao Li, Zhikun Han, Wen Zheng, Xiaopei Yang, Yuqian Dong, Shuqing Song, Dong Lan, Xinsheng Tan, and Yang Yu. Experimental realization of noncyclic geometric gates with shortcut to adiabaticity in a superconducting circuit. *Applied Physics Letters*, 118(25):254002, 2021.
- [62] Qing-Xian Lv, Zhen-Tao Liang, Hong-Zhi Liu, Jia-Hao Liang, Kai-Yu Liao, and Yan-Xiong Du. Accelerating geometric quantum gates through non-cyclic evolution and shortcut to adiabaticity. *arXiv preprint arXiv:1903.03397*, 2019.
- [63] Mikhail I Shalaev, Wiktor Walasik, Alexander Tsukernik, Yun Xu, and Natalia M Litchinitser. Robust topologically protected transport in photonic crystals at telecommunication wavelengths. *Nature nanotechnology*, 14(1):31–34, 2019.
- [64] Haoran Xue, Yihao Yang, and Baile Zhang. Topological valley photonics: physics and device applications. *Advanced Photonics Research*, 2(8):2100013, 2021.
- [65] Yihao Yang, Yuichiro Yamagami, Xiongbing Yu, Prakash Pitchappa, Julian Webber, Baile Zhang, Masayuki Fujita, Tadao Nagatsuma, and Ranjan Singh. Terahertz topological photonics for on-chip communication. *Nature Photonics*, 14(7):446–451, 2020.
- [66] Andrea Blanco-Redondo, Bryn Bell, Dikla Oren, Benjamin J Eggleton, and Mordechai Segev. Topological protection of biphoton states. *Science*, 362(6414):568–571, 2018.
- [67] Hamed Abbaszadeh, Michel Fruchart, Wim Van Saarloos, and Vincenzo Vitelli. Liquid-crystal-based topological photonics. *Proc. Natl. Acad. Sci. U.S.A.*, 118(4):e2020525118, January 2021.
- [68] Hongfei Zhu, Ting-Wei Liu, and Fabio Semperlotti. Design and experimental observation of valley-Hall edge states in diatomic-graphene-like elastic waveguides. *Physical Review B*, 97(17):174301, 2018.
- [69] Laura Pilozzi, Francis A. Farrelly, Giulia Marcucci, and Claudio Conti. Machine learning inverse problem for topological photonics. *Communications Physics*, 1(1):57, Sep 2018.
- [70] Rasmus E Christiansen, Fengwen Wang, Søren Stobbe, and Ole Sigmund. Acoustic and photonic topological insulators by topology optimization. In *Metamaterials, Metadevices, and Metasystems 2019*, volume 11080, page 1108003. SPIE, 2019.
- [71] Rasmus E. Christiansen, Fengwen Wang, and Ole Sigmund. Topological insulators by topology optimization. *Phys. Rev. Lett.*, 122:234502, Jun 2019.

- [72] Vittorio Peano, Florian Sapper, and Florian Marquardt. Rapid exploration of topological band structures using deep learning, 2019.
- [73] Cheng He, Xu Ni, Hao Ge, Xiao-Chen Sun, Yan-Bin Chen, Ming-Hui Lu, Xiao-Ping Liu, and Yan-Feng Chen. Acoustic topological insulator and robust one-way sound transport. *Nature Physics*, 12(12):1124–1129, Dec 2016.
- [74] Zongliang Du, Hui Chen, and Guoliang Huang. Optimal quantum valley Hall insulators by rationally engineering Berry curvature and band structure. *Journal of the Mechanics and Physics of Solids*, 135:103784, February 2020.
- [75] Hai-Xiao Wang, Li Liang, Bin Jiang, Junhui Hu, Xiancong Lu, and Jian-Hua Jiang. Higher-order topological phases in tunable C_3 symmetric photonic crystals. *Photon. Res.*, 9(9):1854, September 2021.
- [76] Yafeng Chen, Fei Meng, Jie Zhu, and Xiaodong Huang. Inverse design of second-order photonic topological insulators in C_3 -symmetric lattices. *Applied Mathematical Modelling*, 102:194–206, February 2022.
- [77] Yafeng Chen, Fei Meng, Yuri Kivshar, Bao-hua Jia, and Xiaodong Huang. Inverse design of higher-order photonic topological insulators. *Phys. Rev. Research*, 2(2):023115, May 2020.
- [78] Cyrill Bösch, Tena Dubček, Frank Schindler, Andreas Fichtner, and Marc Serra-Garcia. Discovery of topological metamaterials by symmetry relaxation and smooth topological indicators. *Physical Review B*, 102(24):241404, 2020.
- [79] XY Long, C Jiang, and X Han. New method for eigenvector-sensitivity analysis with repeated eigenvalues and eigenvalue derivatives. *AIAA journal*, 53(5):1226–1235, 2015.
- [80] Benoit Chachuat. Nonlinear and dynamic optimization: From theory to practice. Technical report, 2007.
- [81] Tae Hee Lee. Adjoint method for design sensitivity analysis of multiple eigenvalues and associated eigenvectors. *AIAA journal*, 45(8):1998–2004, 2007.
- [82] Michael Hinze, René Pinnau, Michael Ulbrich, and Stefan Ulbrich. *Optimization with PDE constraints*, volume 23. Springer Science & Business Media, 2008.
- [83] Andreas Fichtner. *Full seismic waveform modelling and inversion*. Springer Science & Business Media, 2010.
- [84] Martin Philip Bendsoe and Ole Sigmund. *Topology optimization: theory, methods, and applications*. Springer Science & Business Media, 2013.
- [85] Tosio Kato. On the adiabatic theorem of quantum mechanics. *Journal of the Physical Society of Japan*, 5(6):435–439, 1950.
- [86] Jun John Sakurai and Eugene D Commins. *Modern quantum mechanics, revised edition*. American Association of Physics Teachers, 1995.
- [87] Max Born and Vladimir Fock. Beweis des adiabatenatzes. *Zeitschrift für Physik*, 51(3-4):165–180, 1928.
- [88] Cyrill Bösch, Andreas Fichtner, and Marc Serra-Garcia. Differences between quantum and classical adiabatic evolution. *Physical Review B*, 110(6):064307, 2024.
- [89] Toshikaze Kariyado and Yasuhiro Hatsugai. Hannay angle: Yet another symmetry-protected topological order parameter in classical mechanics. *Journal of the Physical Society of Japan*, 85(4):043001, 2016.
- [90] Joseph Samuel and Rajendra Bhandari. General setting for Berry’s phase. *Physical Review Letters*, 60(23):2339, 1988.
- [91] Raphaël Leone. On the parallel transport in quantum mechanics with an application to three-state systems. *arXiv preprint arXiv:1903.04928*, 2019.
- [92] Shivaramakrishnan Pancharatnam. Generalized theory of interference and its applications. 44(6):398–417, 1956.
- [93] Andreas Fichtner. Lecture notes on inverse theory, Cambridge Open Engage, 10.33774/coe-2021-qqq2j, 2021.
- [94] Ya-Wen Tsai, Yao-Ting Wang, Pi-Gang Luan, and Ta-Jen Yen. Topological phase transition in a one-dimensional elastic string system. *Crystals*, 9(6):313, 2019.
- [95] Meng Xiao, ZQ Zhang, and Che Ting Chan. Surface impedance and bulk band geometric phases in one-dimensional systems. *Physical Review X*, 4(2):021017, 2014.
- [96] Neil W Ashcroft, N David Mermin, et al. *Solid state physics*, 1976.

- [97] Heiner Igel. *Computational seismology: a practical introduction*. Oxford University Press, 2017.
- [98] J Zak. Berry's phase for energy bands in solids. *Physical review letters*, 62(23):2747, 1989.
- [99] Kenneth G Wilson. Confinement of quarks. *Physical review D*, 10(8):2445, 1974.
- [100] Frank Wilczek. Introduction to quantum matter. *Physica Scripta*, 2012(T146):014001, 2012.
- [101] Hai-Xiao Wang, Guang-Yu Guo, and Jian-Hua Jiang. Band topology in classical waves: Wilson-loop approach to topological numbers and fragile topology. *New Journal of Physics*, 21(9):093029, 2019.